RSC Advances

PAPER

View Article Online
View Journal | View Issue

Cite this: *RSC Adv.*, 2022, **12**, 13209

Hydroxyapatite formation in biomimetic synthesis with the interface of a pDA@SIS membrane

Qiuhong Zhu,[a] Hua Jiao,[ab] Xiaoliang Zhao,[a] Yufei Tang,[ab] Kang Zhao*[ab] and Xingchun Gou*[c]

Porcine decellularized small intestine submucosa (SIS) is a collagen membrane, which offers great potential as an organic substrate template in mineralization processes due to its good biodegradability and biocompatibility. However, a long period of mineralization and low efficiency are apparent, and the mechanism of collagen fiber mineralization has often been neglected in the previous literature. Thus, in this paper, we present a novel model of biomimetic collagen mineralization which uses dopamine (DA) molecules with the activating and retouching function of SIS collagen membranes and regulating collagen mineralization to construct the structure of mineralized collagen hard tissues. The crystal biomimetic mineralization growth of calcium phosphate on membranes is studied in different solid–liquid interfaces with a double ion self-assembled diffusion system under the simulated physiological microenvironment. In the system, pDA@SIS membranes are used to control the concentration of Ca^{2+} and PO_4^{3-} ionic diffusion to generate supersaturation reaction conditions in 1–14 days. The system can successfully obtain polycrystals with low crystallinity on the pDA-collagen complex template surface of collagen fibers and along the collagen fibers. It initiates a generalized bionic mineralization pathway which can reduce the nucleation interfacial energy to promote rapid hydroxyapatite (HAP) nucleation and crystallization and accelerate the rate of collagen fiber mineralization. The pDA@SIS mineralized collagen membrane shows good biocompatibility with 100% cellular activity in the CCK-8 test, which significantly improved the adhesion proliferation of MC3T3-E1 cells. The pDA-SIS collagen complex, as a new type of mineralization template, may propose a new collagen mineralization strategy to produce a mineralized pDA@SIS scaffold bone-like material for tissue engineering or can potentially be applied in bone repair and regeneration.

Received 11th February 2022
Accepted 22nd April 2022

DOI: 10.1039/d2ra00910b

rsc.li/rsc-advances

1. Introduction

In recent years, an important advance in biomimetic mineralization is the recognition of the regulatory role of organic templates on inorganic minerals. Organic macromolecules play an important role in nucleation, growth and orderly assembly of crystals, which can help the crystals through interfacial recognition and regulation of microstructures. Hard tissues (bone, dentin, enamel, shell, *etc.*) are their own products of biomineralization, and the inorganic phase of the mineralized tissue component is mainly hydroxyapatite, and the other organic phase is mainly type I collagen. Hydroxyapatite crystals are deposited in an orderly manner on the fiber surface or in the interstices under the precise control of collagen molecules, forming a multilevel structure of bone tissue.[1,2] The application of biomimetic mineralization synthesis technology to bone tissue engineering and bone replacement material research provides a new perspective for the construction of tissue-engineered bone with similar morphology, structure *in vitro* and function to natural bone.[3,4] The constructed organic templates provide a site for inorganic nucleation and growth, and use the two-phase interface between inorganic and organic materials to maintain their growth process, which can prepare high biomimetic performance organic/inorganic mineralized collagen based bone repair composites. It is an important topic in the development of new biomaterial science applications today.

Nowadays, the key of research is the design and selection of organic templates,[5] for example, egg-white protein,[6,7] biodegradable plant proteins[8,9] and fibers and polysaccharides were used as bio-templates. However, there are many drawbacks in these templates which need to be further improved, such as poor biocompatibility, potential disease transmission, and high price. Porcine decellularized small intestine submucosa (SIS, a natural extracellular matrix derived material) is obtained by

[a]*School of Materials Science and Engineering, Xi'an University of Technology, Xi'an 710048, China*

[b]*Shaanxi Province Key Laboratory of Corrosion and Protection, Xi'an University of Technology, Xi'an 710048, PR China. E-mail: kzhaocn@gmail.com; Fax: +86029 82312315; Tel: +86029-82312799*

[c]*Institute of Basic Medical Sciences, and Shaanxi Key Laboratory of Brain Disorders, Xi'an Medical University, Xi' an 710021, China. E-mail: go@xiyi.edu.cn; Fax: +86029 86177603; Tel: +86029-86177556*

standard procedures[10] and has been approved by the FDA for tissue repair, and is now widely used for the repair of various soft tissues such as blood vessels, bladder, and skin.[12,13] The use of SIS materials as bone tissue engineering scaffold materials has been reported at home and abroad, and experimental studies have confirmed that SIS matrix membrane has a good porous structure, excellent biocompatibility, biodegradability and mechanical properties.[14] These characters can promote the bone regeneration process effectively.[15,16] In addition, its main components are type I collagen and various cytokines, which are similar to the main organic components of bone.[11,17] Dopamine (DA), as a derivative of adhesion proteins, has received great attention in the field of material surface modification.[18,19] Various substrates exhibit strong adhesion properties which can self-polymerize under light-protected conditions and initiate a generalized bionic mineralization pathway, namely dopamine-assisted HA formation.[20] The reports indicate that materials complexed with dopamine are hydrophilic and promote cell adhesion migration, proliferation and cellular activity.[21,22]

In this thesis, the SIS membrane was modified with dopamine activation to construct pDA-SIS complex membrane as an organic collagen bio-template. The bone-like calcium apatite crystals are successfully biomineralized and synthesized in calcium and phosphorus supersaturated liquid. Mineralized inorganic is self-assembled different membrane–liquid interface double ion diffusion system devices *in vitro* physiological microenvironment. This study provides a theoretical basis for bone formation mechanism, in order to construct new high bionic performance engineered bone-pDA@SIS mineralized collagen-based bone substitute materials. It offers potential application possibilities for bone repair and regeneration.

2. Experimental

2.1 Materials

Calcium acetate($Ca(CH_3COO)_2$,Tianjin Chemical Reagent Factory, China),dipotassium hydrogen phosphate(K_2HPO_4,-Tianjin Chemical Reagent Factory, China), TritonX-100(CP, Xi long Science Co., Ltd),dopamine hydrochloride(98%, Sinopharm Chemical Reagent Co., Ltd), Tris–HCl (>99%, Shanghai Lan ji Biological) *etc.* All other reagents are of analytical grade and can be used without further purification.

2.2 Preparation of SIS and pDA@SIS membrane

After preliminary experiments were carefully carried out, SIS organic collagen matrix membrane was prepared by an optimized decellularization process, mechanical treatment, degreasing, decellularization, sterilization with acetic acid, combined with vacuum freeze-drying method. After lyophilization, the membrane was sterilized and encapsulated at −20 °C for storage. Dopamine-Tris buffer solution (pH = 8.5) was prepared at a mass concentration of 2 mg mL^{-1}, and then submerge the samples in solution. The reaction for 12 h was shaken and mixed on a constant temperature shaker at room temperature, protected from light and normoxic conditions, and ddH_2O was washed three times for 10 min each time to obtain pDA@SIS membranes to dry and sterilize.

2.3 Synthesis of SIS and pDA@SIS mineralized collagen membrane

Fig. 1 shows the solid–liquid interface double ion diffusion and bionic mineralization self-assembly system which simulated bone mineralization conditions (37 °C, pH = 7.4, SIS and pDA@SIS organic collagen matrix membrane as bio-template) and the mineralization reaction process was carried out without stirring. A certain amount (15 mL) of 0.1 M K_2HPO_4 solution was measured and sealed in a polyethylene plastic bottle, and the weighed SIS and pDA @SIS film (3.5 cm × 3.5 cm) was laid flat at the mouth of the bottle and fixed, and then a certain amount(25 mL)of $Ca(CH_3COO)_2$ solution was placed in a small beaker, as shown in Fig. 1 for assembly. The mineralized films were removed after 1, 3, 7 and 14 days respectively, rinsed the surface gently with RO and then put it into an ultrasonic cleaner (25 kHz, 100 W) for 1 min and then lay it flat on a glass slide, coverslip lightly pressed and dried at 37 °C for 24 h for backup. Calcium and phosphorus mineralization solutions 0.2 M and 0.3 M were prepared according to the above method for mineralized collagen films. By controlling the different concentrations of Ca^{2+} in the mineralization solution and the mineralization deposition time, as well as the variation of the self-assembly settings, more uniform and different surface morphologies of bone-like apatite products were quickly obtained.

2.4 Characterization and parameter process optimization

The phase structure of the thin films and crystal samples were carried out on a X-ray spectrometer (XRD-7000, SHIMADZU,

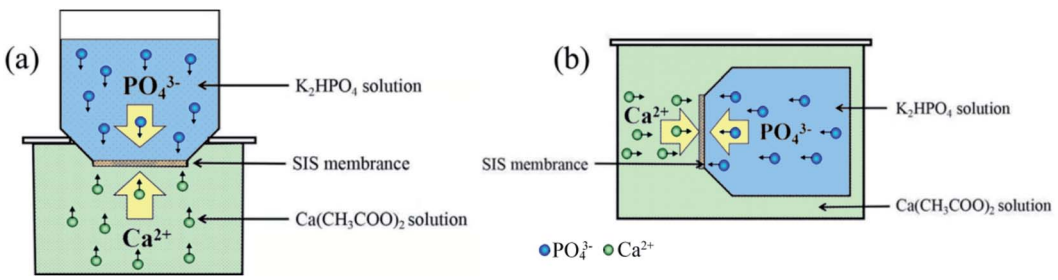

Fig. 1 Schematic diagram of the dual ion diffusion self-assembly system on membrane (a) vertical group (V); (b) level group (L).

Shimadzu, Japan, Cu Kα radiation, 2θ was from 10° to 80°); FTIR analyzed the main components of the membranes and mineralized collagen films; X-ray photoelectron spectroscopy (XPS, ESCALAB 250Xi, Inc. Thermo Fisher USA) analyzed the changes in elemental composition and content after mineralization; the internal microscopic morphology and the degree of mineralization and crystalline phase of the film and mineralized collagen were observed on a SEM (JSM-6700F, JEOL, Japan) and high-resolution transmission microscopy (TEM-3010, Nippon Electron Corporation).

2.5 *In vitro* cell culture

MC3T3-E1 S14 cell (Mouse Pre-cranial Osteoblast Subclone 14, Procell, China) was cultured in α-MEM complete medium containing 10% (v/v) fetal bovine serum (FBS) at 37 °C (5% CO_2) in an incubator, and the medium was changed every 2 days. When the cell growth density reached 80–90%, cells were separated with 0.25% Trypsin–EDTA (Gibco) and made into cell suspensions, which were passaged 1 : 3 for 3–4 days. The cells could be passaged or grown, and the 3rd and 4th generation was selected for subsequent *in vitro* cell experiments; live cells were counted by hemocytometer and diluted with culture medium containing 10% FBS. The final density of cells was determined by subsequent experimental analysis.

2.6 *In vitro* proliferation and cytotoxicity

Biological samples were prepared as circles with a diameter of 6 mm and used as cell culture samples. The groups of materials were placed in 24-well culture plates with 3 parallel samples per group and the test was repeated 3 times. The experimental samples were irradiated with UV light for 30 min on both front and back sides, soaked in 75% ethanol overnight, washed repeatedly with excess sterile PBS to remove the residual ethanol, and the PBS was completely aspirated and discarded; transferred to 96-well culture plates, and the medium was completely aspirated and discarded after being fully soaked with cell culture medium for 12 h. After each group of samples and cells (2×10^3 cell in α-MEM with 10% fetal bovine serum) were co-cultured for 24 h, 48 h and 72 h, cells were washed with PBS buffer for three times, and 100 μL of CCK-8 working solution was added to each well protected from light and incubated for 2 h at 37 °C.[23] Blank wells (medium or PBS) were zeroed and placed in an enzyme marker to measure the A value at 450 nm (after 15 min of shaking at constant temperature), and the relative growth rate (RGR) of cells was calculated according to the formula, the relative cell proliferation rate = average A value of experimental group/average A value of control group × 100%, and the relative proliferation rate of each group was calculated. The larger the RGR is, the less toxic the materials has. The toxicity level above 99 is considered non-toxic and biocompatible.[24]

3. Results and discussion

3.1 Characterization of SIS collagen membrane

SIS collagen organic matrix membrane with translucent shape and translucent shape was obtained after multi-step treatment by physical and chemical methods, and the lyophilized with uniform thickness. The p-SIS film was observed by HE and Masson staining under light microscope as shown in Fig. 2(a and b): there was no residual cell debris on the surface and collagen fibers were undamaged; the cell detachment and fiber arrangement of the SIS collagen membrane(10 mm × 10 mm) were observed in Fig. 2(c and d) that the collagen fibers were tightly arranged, but their internal structure was loose and consisted of multiple nanoscale fine fiber bundles. There were finer fiber connections between the fiber bundles, and the fiber arrangement was reticulated, no residual cell morphology was

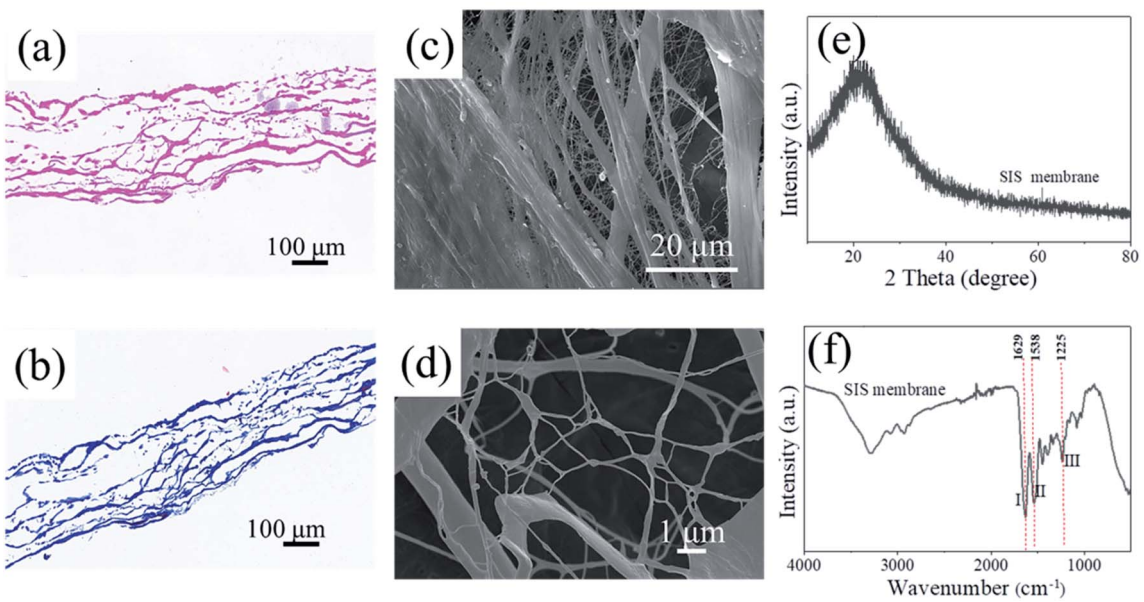

Fig. 2 Components of SIS membrane (a) no cell nucleus; (b) col components and (c and d) SEM image; (e) XRD spectra; (f) FTIR spectra.

seen. The pores between the fiber bundles were obvious, the collagen fiber network was not damaged. The natural network structure of collagen was retained and the collagen was moderately loosened. It can be seen that SIS has a three-dimensional mesh structure with interconnected pores, and is an extracellular matrix material without cells, which is non-antigenic and does not cause significant immune rejection as an *in vitro* mineralized biological template, laying the foundation for subsequent experiments.

Fig. 2(e) shows XRD pattern that SIS has a characteristic diffraction peak with low intensity and high half-peak width at 21.39°, which is a non-crystalline material resulting in a diffuse broad peak; Fig. 2(f) shows FTIR spectra that the extracted SIS collagen membrane has three characteristic peaks of amide bond-I (1629 cm^{-1}, C=O stretching vibration peak), II (1538 cm^{-1}, N–H surface inward bending vibration peak and C–H stretching vibration peak), and III (1225 cm^{-1}, C–N stretching vibration peak and N–H surface inward bending vibration peak), which demonstrate that the functional group position of the extracted porcine small intestine submucosa matrix membrane is consistent with the type I collagen functional group.[25] The molecular structure of type I collagen was protected during the extraction process, and the microstructure remained stable and maintained the original structure and biological activity of collagen, which was in accordance with the required standards for subsequent experiments.

3.2 XRD, FTIR analysis

The phase composition of the pDA@SIS and SIS collagen mineralization crystal products are characterized as shown in Fig. 3. The intensity of HA characteristic diffraction peaks are corresponding to 25.9°, 31.7° and 32.1°, and 32.9° all became higher as shown in Fig. 3(a–f), with diffraction peaks corresponding to (002), (211), (112) and (300) crystal planes. In addition, the intensity of the characteristic diffraction peaks at 16.8° (101), 22.8° (111) and 49.2° (213) corresponding to HA growth significantly with increasing concentration and mineralization time. Fig. 3(a and d) shows that the XRD patterns of the 1 d samples are confirmed as calcium phosphate dehydrate ($CaHPO_4$–$2H_2O$, DCPD. PDF: 09-0077) and hydroxyapatite (HAP. PDF: 09-0432) mixture; after modification and mineralization for 3 d or above, the main product is identified as HAP, indicating that most of the DCPD has been converted to HAP by the mineralization reaction, and the diffraction pattern of anisotropic HAP matches well with the standard XRD pattern spectrum of unoriented HAP with high similarity[26,27] and deposition rate plus; however, the diffraction peak intensity is relatively weak, which can be considered to be caused by the difference in mineralization product content, proving that both bone-like apatites are weakly crystalline HA crystals and have imperfect crystal structures; and compared to the chemically synthesized standard, both are a diffraction peak with a wide base, large span, low intensity, and not sharp peak shape, while the (300) diffraction peak is not obvious, indicating that the mineralized film crystal product bone-like apatite is in a weak crystalline state, indicating that the crystallinity becomes lower or the crystal volume decreases. It was shown that low crystallinity enhances the expression of osteogenesis-related genes.[28] Therefore, this matrix membrane mineralized HAP has the potential to induce bone repair. This feature is similar to the

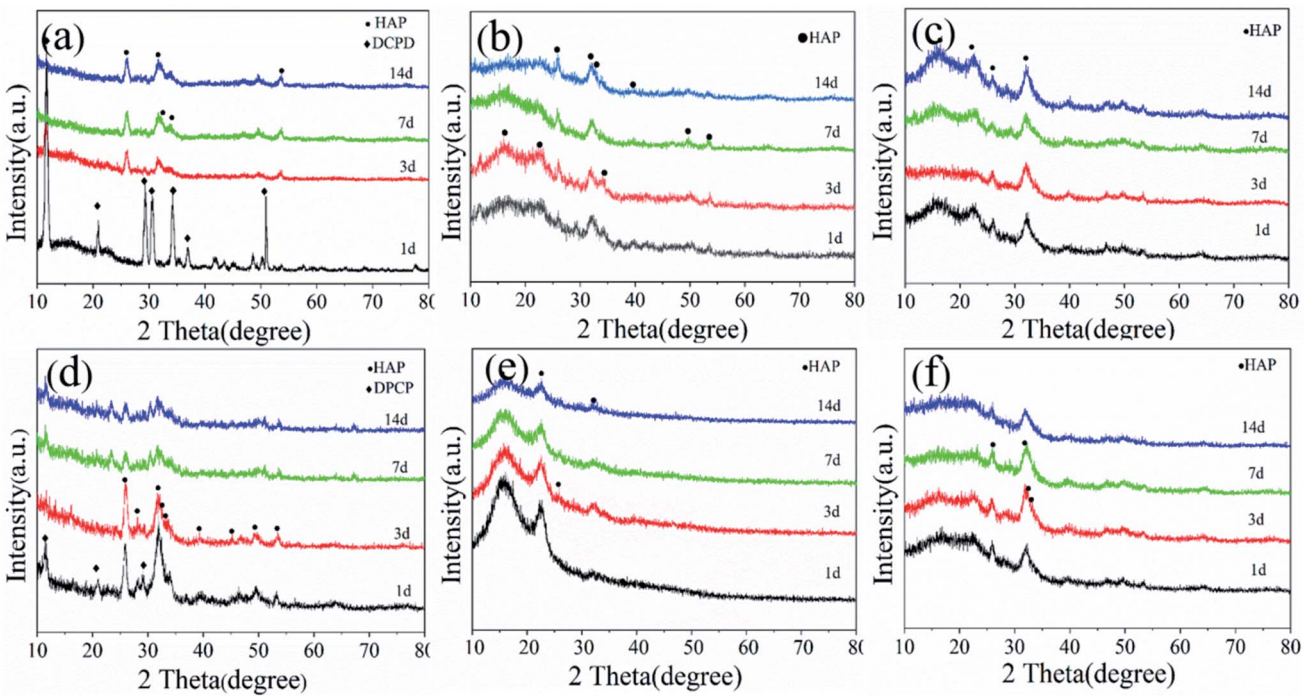

Fig. 3 XRD spectra of pDA@SIS (a–c) and SIS mineralized collagen membrane (d–f) in different concentrations Ca^{2+}(a and d-0.1 M; b and e-0.2 M; c and f-0.3 M)at different mineralization times(1–14 d) under vertical group.

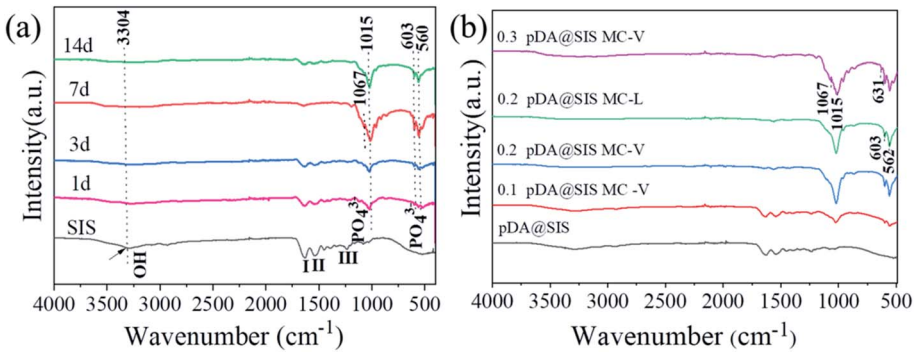

Fig. 4 IR patterns of samples (a) SIS and SIS mineralized collagen membranes at different holding times 1–14 d by 0.2 M Ca^{2+} under vertical group; (b) pDA@SIS mineralized collagen membranes at mineralization 3 d for different Ca^{2+} concentrations under devices: V and L.

apatite crystals of natural bone, and the main phase of the product is HAP, with the most pronounced diffraction peaks around $2\theta = 25.9°$ and 31.7° in all groups. Human mineralized tissues are mainly composed of calcium phosphates, the most common being apatite, represented by hydroxyapatite (HAP), and to a lesser extent octacalcium phosphate (OCP), calcium phosphate dihydrate ($CaHPO_4$–$2H_2O$, DCPD)/tricalcium phosphate (α/β-TCP),[29] which differ mainly by their Ca/P molar ratio, Ca^{2+} carboxylation, and PO_4^{3-} protonation. These mineral salts are related to each other and under certain conditions they can be transformed into each other in order to adapt to the needs of the biological matrix.

FTIR spectrograms characterizing the functional groups of different samples of mineralized collagen are shown in Fig. 4. The peak intensities of amide I, II, and III of mineralized collagen are observed in both Fig. 4(a and b) to decrease significantly after mineralization to the extent that the amide II peak almost disappears; the decrease in the intensity of the amide I peak is mainly due to the blockage of C=O stretching.[30] In addition, the peak of amide I gradually shifts to a lower wave number during collagen mineralization. It can be inferred that the bonding of the two occurred during mineralization, indicating that the greater content of apatite material covering the surface of collagen micro-fibrils masked the vibrational peaks of collagen. The results above indicated that HAP was generated by deposition on the SIS and pDA@SIS matrix membranes. Combined with the XRD test results, we can conclude that products of pDA@SIS collagen membranes were deposited more and mineralized faster. The characteristic absorption peaks at 560, 603, 1015, 1067 cm^{-1}, and 3304 cm^{-1} were observed in Fig. 4(a and b) showed PO_4^{3-}salt bending vibrational peak and vibrational absorption peak at (562, 631, 1042 and 1104 cm^{-1}), vibrational absorption peak at (3304 cm^{-1}) corresponds to the functional group –OH which associated with the water absorption of mineralized collagen.[16,31] The results indicate the presence of mineral particles.

3.3 SEM analysis

3.3.1 SEM morphology analysis of the products with different ion concentration and mineralization time. The morphology of CaP crystals generated on pDA@SIS collagen membranes are shown in Fig. 5. They change dramatically compared with the original surface morphology at different concentrations as shown in Fig. 5(a1–c1) at mineralization time 1 d. With the increase of mineralization time, a large number of white particles were produced on the film surface, and the new layer grew well that was completely covered uniformly in mineralization time 3 d in Fig. 5(a2–c2). The gravity was assembled by dissolution crystallization layer by layer during the crystal growth process, forming a uniform dense layer of the two-dimensional lamellar structure which was assembled into a special petal-like structure; some of them were assembled into a sphere-like nanoscale porous structure in the three-dimensional lattice of the SIS films at reaction time 7 d in Fig. 5(a3–c3). These spherical deposits consisted of a large number of lamellar crystals with piled up at the edges and exfoliated in the center, and the exfoliated exposed swollen collagen fibers were visible, while the deposits were seen to grow in the direction of the collagen fibers in Fig. 5(a4–c4). The crystals show a variety of shapes, lamellar, petal-like or spherical. Nucleated growth on lamellar HAP showed a three-dimensional porous structure, providing some space for cell growth. Studies have reported that HAP in natural bone tissues are ultrathin lamellar structures, and many researchers have prepared such lamellar HAP *in vitro* mineralization, a typical morphology.[32]

With the increase of calcium ion solution concentration (0.1–0.3 M), some areas are single layer of powder particles and others are multi-layer particles on the films of the various thickness by influenced gravity factors. The mineralization products exist edge accumulation and central exfoliation phenomenon, especially high concentration in Fig. 5(c1–4) show a large number of mineralization products filling in the three-dimensional network of SIS films. Combination with XRD and IR tests, the process of 0.2 M Ca^{2+} was chosen for the subsequent experiments, which were more favorable to the ion diffusion process and also to the crystallization growth of bone-like calcium phosphate.

3.3.2 Analysis of mineralized film morphology and structure by ion diffusion self-assembly modepDA@SIS. Fig. 6(a and b) shows the collagen mineralized film morphology and Ca–P crystal structure with the effect of gravity-free factor. White

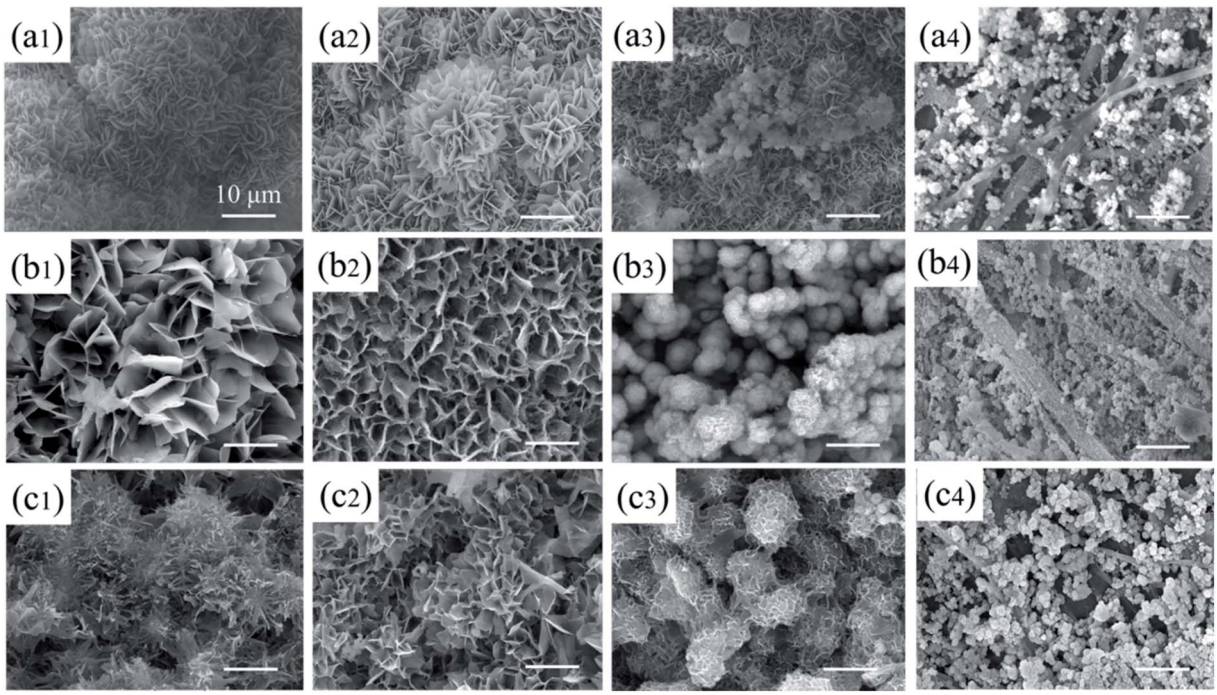

Fig. 5 Morphology of pDA@SIS mineralized collagen membranes under V group obtained different Ca^{2+} concentrations (a-0.1 M, b-0.2 M, c-0.3 M)and mineralization times(1-1 d, 2-3 d, 3–7 d, 4–14 d).

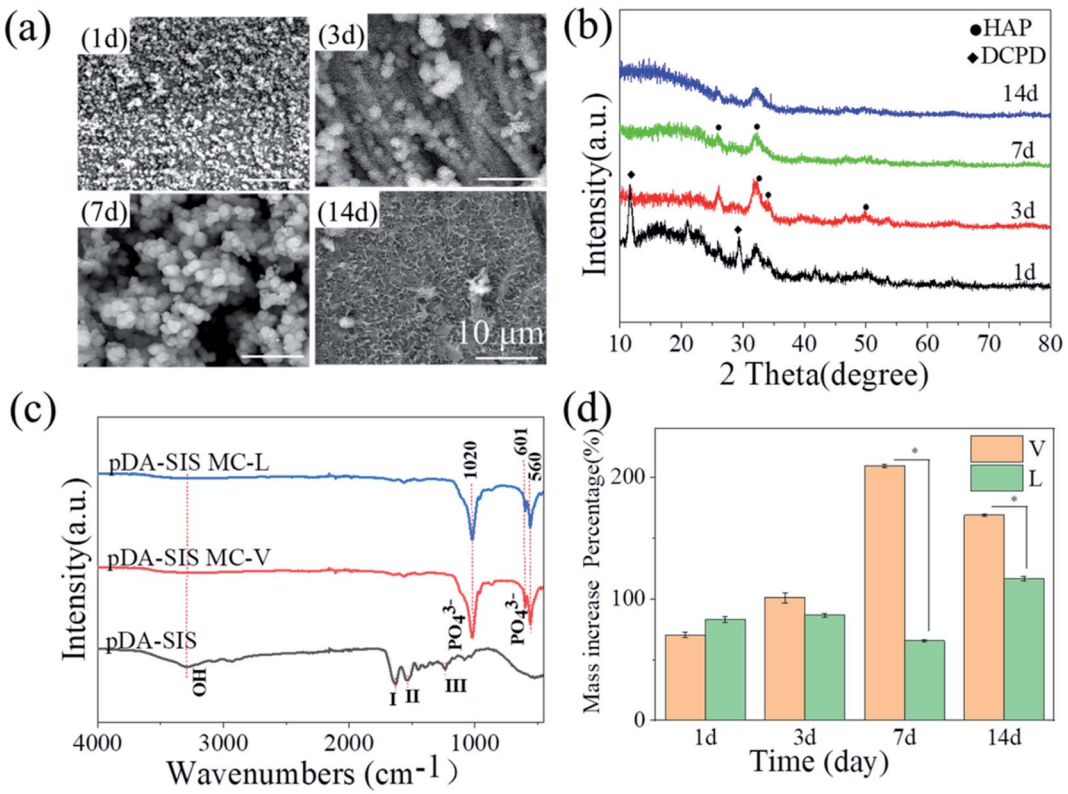

Fig. 6 (a) Morphology of pDA@SIS mineralized collagen films and (b) XRD pattern (Ca^{2+}: 0.2 M under L group, different mineralization time: 1 d, 3 d, 7 d, 14 d); (c) IR pattern(Ca^{2+}: 0.2 M, mineralization time: 3 d, V–L group); (d) Mass increase percentage histogram of apatite mineralized sediment (Ca^{2+}: 0.2 M, mineralization time 1 d, 3 d, 7 d, 14 d, V/L group).

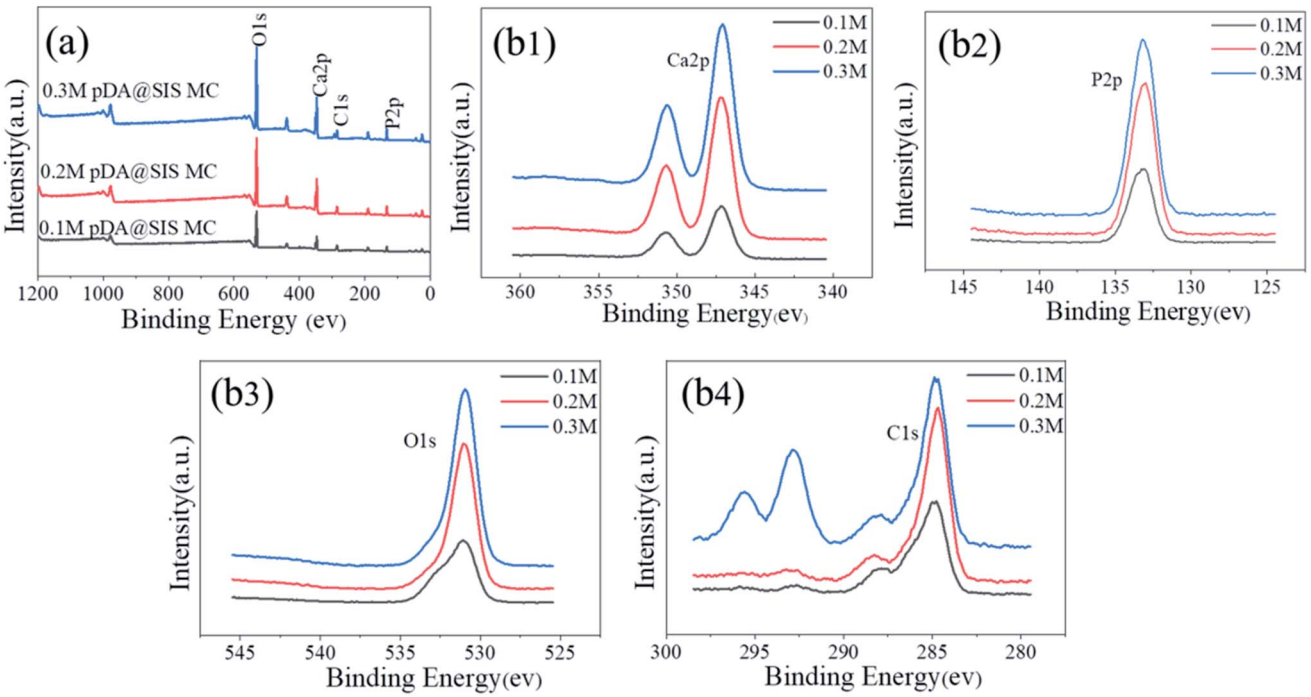

Fig. 7 (a) The XPS full scan spectra of PDA@SIS mineralized collagen membranes obtained at mineralization time 3 d with different Ca^{2+} concentrations; (b1) P 2p region; (b2) Ca 2p region; (b3) C 1s region; (b4) O 1s region.

particle crystals partially covered the collagen film at holding time 1–3 d; with the increase of time, HAP growth process of the L-group has less edge stacking phenomenon, forming an inhomogeneous particle layer. The deposition amount first increased and then decreased as shown under groups at different mineralization times in Fig. 6(d). It can be seen that the weight gain of the vertical group is slightly higher at same time.

XRD pattern in Fig. 6(b) shows that the samples were identified as a mixture of DCPD and HAP at 1 d and the main product was identified as HAP at 3 d. It indicates that most of the DCPD has been converted to HAP by bionic mineralization reaction, with each group at $2\theta = 25.9°$ (002), 31.7° (211) and 49.2° (213) are more pronounced diffraction peaks. Consistent with the HAP (HAP, PDF: 09-0432), the rapid synthesis of HAP on the pDA@SIS membrane both horizontally and vertically was demonstrated. IR mapping in Fig. 6(c) shows PO_4^{3-} bending vibrational absorption peaks at ($\nu \sim 560$ and 601 cm^{-1}; $\nu \sim 1020$ cm^{-1}) at mineralized 3 d of the 0.2 M V–L groups, confirming the deposition of calcium apatite too.

3.4 XPS, TEM analyses

Fig. 8(a) is a TEM photograph that the like-flowers porous the synthesized crystals on the pDA@SIS surface which are in the form of elongated lamellae with a width of about 30–50 nm and a thickness of about 10–20 nm; Fig. 8(b) is the HRTEM photograph corresponding to (a). It was calculated from the lattice phase data that the crystalline spacing is 0.344 nm which corresponds to the face spacing value of the (002) crystalline plane of the hexagonal phase HAP. Thus the synthesized HAP crystals prepared after dopamine modification is finer and more

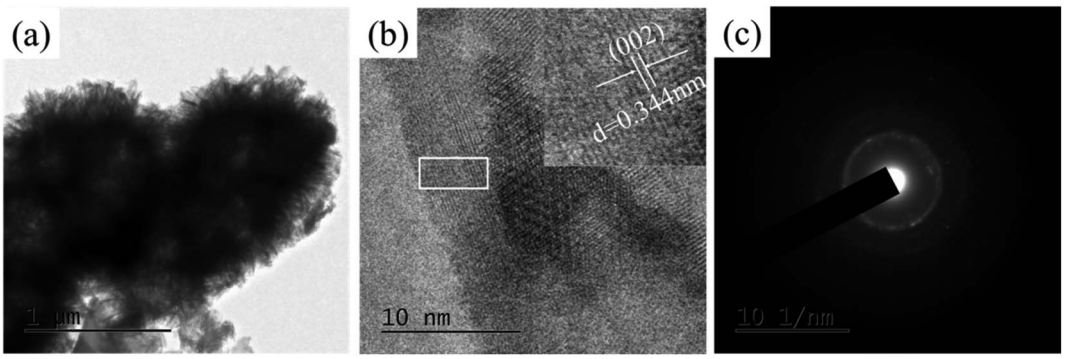

Fig. 8 (a) TEM images of samples at 0.2 M Ca^{2+} for 3 d; (b) HRTEM image; (c) SAED image.

suitable for the study of bone repair. This is further illustrated by the diffraction pattern in Fig. 8(c) which shows a SAED photograph with a circular bright streak image where two diffraction rings represent the (002) and (112) facets of the weakly crystalline HAP. The crystals are a polycrystalline structure. The above results indicate that the HAP nanosheets are rapidly grown on pDA@SIS organic collagen membrane by the biomimetic mineralization method.

In order to further characterize the differences of Ca (2p) peak, P 2p peak, C 1s peak and O 1s peak on the surface of mineralized collagen, Fig. 7(a and b) shows a peak splitting process that the mineralized film contains Ca, P, O, and C. The binding energies of Ca (2p) are 347.2 and 358.1 eV respectively; the binding energies of P 2p is 133.2 eV; the binding energies of O 1s is 531.74 eV and the binding energies of C 1s are 285.3 and 293.1 eV respectively. The above results show that the calcium apatite was successfully obtained on the pDA@SIS collagen membrane by biomimetic mineralization synthesis. Based on the results of the corresponding elemental content analysis, the distribution of the components in the product was determined by comparing the peaks of the major elements P and Ca in the components according to the composition membrane. With the gradual increase of Ca^{2+}concentration from 0.1 M to 0.3 M, it is concluded that the Ca/P ratio of the sediment in the product increases and then decreases. XPS spectra of samples after 3 d mineralization with 0.2 M Ca^{2+}, nCa/P = 1.60 which is slightly smaller than the ratio of human bone HAP.

3.5 Analysis of mineralization formation process and mechanism

In this process, in addition to the previously reported nucleation sites of carboxyl (–COOH) and carbonyl (–C=O) on collagen, there is another nucleation site, *i.e.*, the protonated amino NH_2 is slowly neutralized by the generated hydroxyl groups and some excess hydroxyl OH is adsorbed to the surface of pDA@SIS resulting in a negative charge on the surface of the pDA@SIS collagen membrane. In the initial stage, Ca^{2+} and $(HPO_4)^{2-}$ diffuse from different sides of the surface of the dopamine-modified SIS membrane, which is more prone to precipitate generation because of the enriched functional groups in these regions. The free Ca^{2+} in solution is electrostatically enriched and adsorbed to the collagen membrane providing a template and regulatory role in determining the crystallization mode and size of the mineral. These calcium phosphate crystals of anisotropic act as nucleation sites to induce further crystallization of inorganic material, eventually completing the mineralization process quickly. The inset also clearly shows this structural feature of the mineralized product, *i.e.*, bone-like apatite as shown in XRD Fig. 3 and similar morphology can also be observed from SEM Fig. 5 and 6(a) and TEM Fig. 8(a). Combined with the above morphological analysis results and kinetic studies, it can be concluded the formation mechanism of mineralization product morphology to form nanosheets after chemical reaction, nucleation and crystal growth. With the extension of mineralization time, the crystals continuously dissolve and recrystallize to form special petal-like morphology and spherical crystals by secondary self-assembly. These pore structure is actually formed by bending and stacking of multilayer calcium phosphate lamellar crystals in Fig. 9. According to the principle of energy minimum of thermodynamic point of view, these irregular lamellas self-assemble into flower-like morphology to reduce the surface energy. pDA@SIS membrane as a biotemplate regulates the mode and the size to provide the growth point of mineral crystallization.

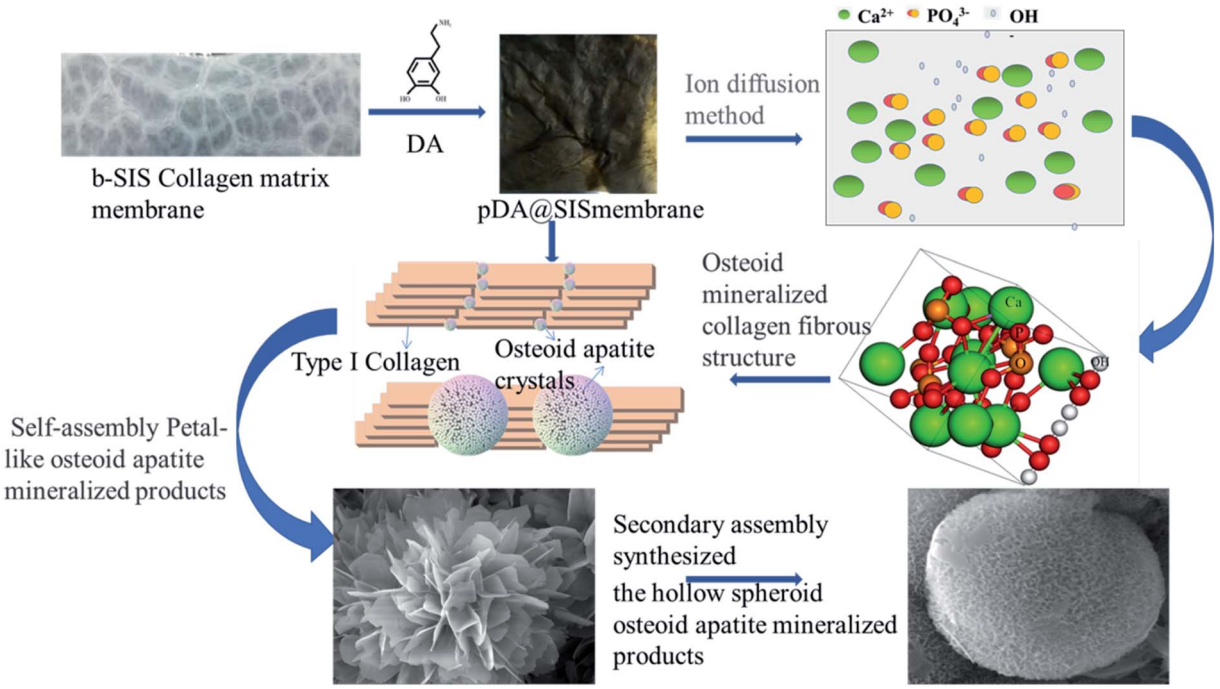

Fig. 9 Schematic diagram of the formation process of bone-like mineralized collagen micro-nanostructures.

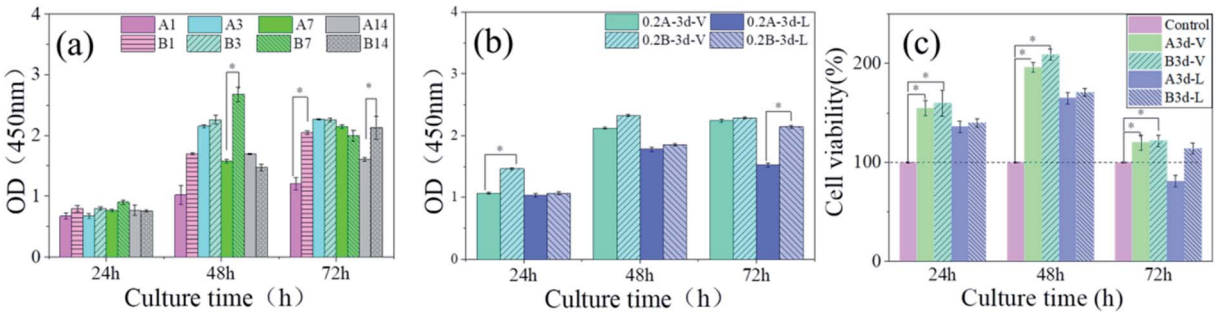

Fig. 10 Proliferation of MC3T3-E1 seeded of different samples for 24, 48 and 72 h by CCK8 assay (* for $P < 0.05$, $n = 3$): (a) SIS and pDA@SIS mineralized membrane (A and B samples from 0.2 M Ca^{2+} at different mineralization times under V); (b) pDA@SIS mineralized membrane the optimized (samples from 0.2 M Ca^{2+} at 3 d under V/L); (c) cell viability test (%).

According to crystal growth theory, vertical growth requires lower energy than planar growth[10,33] and the driving force for apatite crystals self-assembly is the Gibb's free energy of the systematic transition from supersaturation to equilibrium during biomimetic mineralization.[34] Mineralized crystal has a relatively uniform thickness and the propagation of bone mineral is mediated by well-aligned collagen fibers in the extracellular matrix and multiple matrix proteins that affect the nucleation and growth or aggregation of crystals.[35] During biomineralization, the deposition site and growth direction of HAP are governed by the pDA@SIS template, and lamellar HAP formation is consistent with bone biomineralization.[36]

3.6 *In vitro* biocompatibility

Fig. 10 shows CCK-8 cell proliferation tests of MC3T3-E1 S14 osteoblasts in SIS and pDA@SIS mineralized collagen samples co-cultured for 24, 48 and 72 hours respectively. Each group was averaged 3 times and (*) indicates a significant difference ($p < 0.05$). It was repeatedly verified that osteoblast activity was higher at 0.2 M Ca^{2+} concentrations. A study by Maeo *et al.*[37] found that low and medium concentrations of calcium ions are beneficial for osteoblast proliferation and high concentrations can be toxic to the cells. The results are displayed as bar graph of OD-culture time in Fig. 10(a and b) and cell viability (relative growth rate, RGR > 100% in Fig. 10(c)). The results clearly confirmed the pDA@SIS collagen membrane as an organic template for the rapid synthesis of osteoclast-like apatite which is non-toxic and better cell biocompatibility. The adhesion migration and proliferation of the material to cells can be improved. Therefore, subsequent experiments are carried out to prepare samples with 0.2 M Ca^{2+} mineralization time of 3 days under a vertical group.

4. Conclusions

In this study, dopamine is introduced into SIS for activation modification as an organic biological template, and the process of mineralized synthesis of bone-like apatite inorganic material was fabricated without high temperature forging, at 37 °C and near neutral conditions at pH 7.4. The nucleation rate is faster than the unmodified one, indicating that the modification reduced the nucleation interface and its nucleation conforms to the description of classical nucleation theory. The obtained results show that the bionic mineralization method successfully synthesized low crystallinity bone-like HAP polycrystals under the modulation of pDA@SIS collagen membrane, and obtained mineralized collagen-like bone basic unit (MC), which is not toxic to MC3T3-E1 S14 cells. This study explores the importance of using organic membrane pDA@SIS with similar synthesis conditions to the apatite growth environment in human bone, providing a new perspective for the understanding of bone formation *in vivo* and a theoretical basis for the preparation of novel biomimetic pDA@SIS mineralized collagen-based bone graft materials in the future.

Conflicts of interest

The authors declare no potential conflicts of interest with respect to the authorship and/or publication of this article.

Acknowledgements

This work described in this paper was supported by the Natural Science Basic Research Foundation of Shaanxi Province (No. 2020JQ-626) and the National Natural Science Foundation (No. 52172073). The supports of the Youth Innovation Team of Shaanxi Universities (leader: Dr Xingchun Gou) and the Science and Technology Innovation Team of Shaanxi (leader: Dr Xingchun Gou) are highly appreciated.

References

1 J. M. Sadowska, G.-M. Jordi, E. B. Montufar, *et al.*, Biomimetic *versus* Sintered Calcium Phosphates: the *in vitro* Behavior of Osteoblasts and Mesenchymal Stem Cells, *Tissue Eng., Part A*, 2017, **23**, 1297–1309.
2 N. Reznikov, M. Bilton, L. Lari, M. Stevens and R. Krger, *Science*, 2018, **30**, 1503–1510.
3 J. H. Bradt, M. Mertig, A. Teresiak and W. Pompe, Biomimetic mineralization of collagen by combined fibril assembly and calcium phosphate formation, *Chem. Mater.*, 1999, **11**, 2694–2701.

4 X. Li, J. Xie, J. Lipner, X. Yuan, S. Thomopoulos and Y. Xia, Nanofiber Scaffolds with gradations in mineral content for mimicking the tendon-to-bone insertion site, *Nano Lett.*, 2009, **9**, 2765–2768.

5 M. Kikuchi, S. ltoh, S. Ichinose, *et al.*, Self-organization mechanism in a bone-like hydroxyapatite/collagen nanocomposite synthesized *in vitro* and its biological reaction *in vivo*, *Biomaterials*, 2001, **22**, 1705–1711.

6 M. Takiguchi, K. Igarashi, M. Azuma, *et al.*, Flowerlike agglomerates of calcium carbonate crystals formed on an eggshell membrane, *Cryst. Growth Des.*, 2006, **6**, 2754–2757.

7 Y. Zhang, Y. Liu, X. Ji, C. E. Banks and J. Song, Flower-like agglomerates of hydroxyapatite crystals formed on an egg-shell membrane, *Colloids Surf., B*, 2011, **82**, 490–496.

8 C. Y. Zhang, W. Zhang, H. Yao, H. Zhu, L. Mao and S. Yu, Bioinspired crystallization of continuous calcium phosphate films on a langmuir monolayer of zein protein: their mechanical performance, hydrophilicity, and biocompatibility, *Cryst. Growth Des.*, 2013, **13**, 3505–3513.

9 Y. Zhang, Y. Liu and X. B. Ji, Fabrication of flowerlike hydroxyapatite agglomerates with the assistant of bamboo membrane, *Mater. Lett.*, 2011, **65**, 1982–1985.

10 M. Y. Yang, J. Wang, Y. Zhu and C. B. Mao, Bio-templated growth of bone minerals from modified simulated body fluid on nanofibrous decellularized natural tissues, *Biomed. Nanotechnol.*, 2016, **12**, 753–761.

11 K. S. Kim, J. Y. Ju, M. K. Yun, E. S. Kin, *et al.*, Small intestine submucosa sponge for *in vivo* support of tissue engineered bone formation in the presence of rat bone marrow stem cells, *Biomaterials*, 2010, **31**, 1104–1113.

12 G. Khan, H. A. Ko, K.-S. Han, N. K. Jang and J. E. Song, Effect of small intestinal submucosa sponges on the attachment and proliferation behavior of Schwann cells, *Macromol. Res.*, 2014, **22**, 1253–1260.

13 D. M. Sanchez-Palencia, D. '. A. Antonio, A. González-Mancerag, W. R. Wagnerc and J. C. Briceño, Effects of fabrication on the mechanics, microstructure and micromechanical environment of small intestinal submucosa scaffolds for vascular tissue engineering, *J. Biomech.*, 014, **47**, 2766–2773.

14 W. Wu, B. Li, Y. Liu, *et al.*, Effect of multilaminate small intestinal submucosa as a barrier membrane on bone formation in a rabbit mandible defect model, *BioMed Res. Int.*, 2018, **2018**, 1–11.

15 J. C. Luo, W. Chen, X. H. Chen, T. W. Qin, Y. C. Huang, H. Q. Xie, X. Q. Li, Z. Y. Qian and Z. M. Yang, A multi-step method for preparation of porcine small intestinal submucosa(SIS), *Biomaterials*, 2011, **32**, 706–713.

16 M. Y. Yang, G. S. Zhou, H. C. Izquierdo, Y. Zhu and C. B. Mao, Biomineralization of natural collagenous nanofibrous membranes and their potential use in bone tissue engineering, *Biomed. Nanotechnol.*, 2015, **11**, 447–456.

17 S. Bose, M. Roy and A. Bandyopadhyay, Recent advances in bone tissue engineering scaffolds, *Trends Biotechnol.*, 2012, **30**, 546–554.

18 Y. Zeng, W. Liu, Z. Wang, S. Singamaneni and R. Wang, Multifunctional surface modification of nanodiamonds based on dopamine polymerization, *Langmuir*, 2018, **34**, 4036–4042.

19 L. Ge, L. Liu, H. Wei, *et al.*, Preparation of a small intestinal submucosa modified polypropylene hybrid mesh *via* a mussel-inspired polydopamine coating for pelvic reconstruction, *J. Biomater. Appl.*, 2016, **30**, 1385–1391.

20 J. Ryu, S. H. Ku, H. Lee and C. B. Park, Mussel-inspired polydopamine coating as a universal route to hydroxyapatite crystallization, *Adv. Funct. Mater.*, 2010, **20**, 2132–2139.

21 H.-jin Cho, S. K. Madhurakkat Perikamana, *et al.*, Effective Immobilization of BMP-2 Mediated by Polydopamine Coating on Biodegradable Nanofibers for Enhanced *in vivo* Bone Formation, *ACS Appl. Mater. Interfaces*, 2014, **6**, 11225–11235.

22 R. F. Luo, L. L. Tang, J. Wang, Y. C. Zhao, Q. F. Tu, Y. J. Weng, R. Shen and N. Huang, Improved immobilization of biomolecules to quinone-rich polydopamine for efficient surface functionalization, *Colloids Surf., B*, 2013, **106**, 66–73.

23 J. W. Xiong, H. Xiao and Z. X. Zhang, An experimental research on different detection conditions between MTT and CCK-8, *Acta Laser Biol. Sin.*, 2007, **16**, 559–562.

24 T. K. Qiao, P. Song, H. L. Guo, X. F. Song, B. C. Zhang and X. S. Chen, Electrospun PLLA fiber membrane *via* chemical crosslinking, *Eur. Polym. J.*, 2016, **74**, 101–108.

25 T. W. Sun, Y. J. Zhu, F. Chen and Y. G. Zhang, Ultralong Hydroxyapatite Nanowire/Collagen Biopaper with High Flexibility, Improved Mechanical Properties and Excellent Cellular Attachment, *Chem.–Asian J.*, 2017, **12**, 655–664.

26 M. Aizawa, T. Matsuura and Z. Zhuang, Syntheses of single-crystal apatite particles with preferred orientation to the *a*- and *c*-axes as models of hard tissue and their applications, *Biol. Pharm. Bull.*, 2013, **36**, 1654–1661.

27 Y. J. Zhang and J. J. Lu, The transformation of single-crystal calcium phosphate ribbonlike fibres to hydroxyapatite spheres assembled from nanorods, *Nanotechnology*, 2008, **19**, 55608–55617.

28 Y. Li, Y. Wang, Y. Li, *et al.*, Controllable Synthesis of Biomimetic Hydroxyapatite Nanorods with High Osteogenic Bioactivity, *ACS Biomater. Sci. Eng.*, 2020, **6**, 320–328.

29 X. Wang, S. P. Grogan, F. Rieser, V. Winkelmann, V. Maquet, M. L. Berge and P. Mainil-Varlet, Tissue engineering of biphasic cartilage constructs using various biodegradable scaffolds: an *in vitro* study, *Biomaterials*, 2004, **25**, 3681–3688.

30 A. Bigi, E. Boanini, S. Panzavolta and N. Roveri, Biomimetic growth of hydroxyapatite on gelatin films doped with sodium polyacrylate, *Biomacromolecules*, 2000, **1**, 752–756.

31 T. Bian, K. Zhao, Q. Meng, Y. Tang, H. Jiao, J. Luo and X. Liu, Synthesis of plate-like single-crystal hydroxyapatite rods with *c*-axis orientation by biotemplate small intestinal submucosa, *Ceram. Int.*, 2017, **43**, 11807–11814.

32 R. Xin, Y. Lang, J. Chen and Q. Zhang, A comparative study of calcium phosphate formation on bioceramics *in vitro* and *in vivo*, *Biomaterials*, 2005, **26**, 6477–6486.

33 M. Y. Yang, G. S. Zhou, H. C. Izquierdo, Y. Zhu and C. B. Mao, Biomineralization of natural collagenous nanofibrous membranes and their potential use in bone tissue engineering, *Biomed. Nanotechnol.*, 2015, **11**, 447–456.
34 P. Calvert and S. Mann, Synthetic and biological composites formed by *in situ* precipitation, *J. Mater. Sci.*, 1988, **23**, 3801–3815.
35 L. C. Palmer, C. J. Newcomb, S. R. Kaltz, E. D. spoerke and S. I. Stupp, Biomimetic systems for hydroxyapatite mineralization inspired by bone and enamel, *Chem. Rev.*, 2008, **108**, 4754–4783.
36 S. Weiner and P. M. Dove, An overview of biomineralization processes and the problem of the vital effect, *Rev. Mineral. Geochem.*, 2003, **54**, 1–29.
37 A. S. Maeno, A. Y. Niki and A. H. Matsumoto, The effect of calcium ion concentration on osteoblast viability, proliferation and differentiation in monolayer and 3D culture[J], *Biomaterials*, 2005, **26**, 4847–4855.